Chemical Science

ROYAL SOCIETY OF CHEMISTRY

EDGE ARTICLE



Cite this: *Chem. Sci.*, 2024, **15**, 10408

All publication charges for this article have been paid for by the Royal Society of Chemistry

Received 3rd April 2024
Accepted 10th June 2024

DOI: 10.1039/d4sc02206h

rsc.li/chemical-science

# Key structural features to favour imines over hydrates in water: pyridoxal phosphate as a muse†

Ferran Esteve, * Tanguy Rieu and Jean-Marie Lehn *

Imination reactions in water represent a challenge not only because of the high propensity of imines to be hydrolysed but also as a result of the competing hydrate formation through $H_2O$ addition to the aldehyde. In the present work we report a successful approach that allows for favouring imitation reactions while silencing hydrate formation. Such remarkable reactivity and selectivity can be attained by fine-tuning the electronic and steric structural features of the *ortho*-substituents of the carbonyl groups. It resulted from studying the structure–reactivity relationships in a series of condensation reactions between different amines and aldehydes, comparing the results to the ones obtained in the presence of the biologically-relevant pyridoxal phosphate (**PLP**). The key role of negatively-charged and sterically-crowding units (*i.e.*, sulfonate groups) in disfavouring hydrate formation was corroborated by DFT and steric-hindrance calculations. Furthermore, the best-performing aldehyde leads to higher imine yields, selectivity and stability than those of **PLP** itself, allowing for the inhibition of a **PLP**-dependent enzyme (transaminase) through dynamic aldimine exchange. These results will increase the applicability of imine-based dynamic covalent chemistry (DCvC) under physiological conditions and will pave the way for the design of new carbonyl derivatives that might be used in the dynamic modification of biomolecules.

## Introduction

Imine-based dynamic covalent reactions have offered remarkable advantages in a wide range of fields.[1–3] The reversible nature of aldimine covalent bonds allows for thermodynamically-driven dynamic rearrangements and error-checking processes,[4] with the species (or mixture) that presents the lowest free energy predominating in equilibrium under specific conditions.[5–8] Such dynamicity proved useful for the development of systems displaying a behaviour of higher complexity.[9–11] Nevertheless, the high propensity of imines to be hydrolysed in aqueous media has hampered their application under physiological conditions.[12] As a consequence, many research efforts have been devoted in the last years toward the implementation of chemical methods that increase the stability of imines in water, mainly using covalent/supramolecular multivalency and hydrophobic effects.[13–17] In nature, imitation reactions are achieved in the sophisticatedly-arranged active sites of enzymes, using pyridoxal phosphate (**PLP**) as the aldehyde.[18] The mode-of-action of this cofactor has been extensively studied as it plays an essential role in numerous enzymatic processes (*e.g.*, racemizations, transaminations, aldol cleavages, and decarboxylations).[19,20] Briefly, the pyridine ring acts as an electron sink to enhance the electrophilic character of the carbonyl group; the –OH group in *ortho*-position to the carbonyl unit is involved in amine activation and imine stabilization through H-bonding/electrostatic attractions; and the phosphate sidechain mainly acts as the anchoring scaffold to the protein's active site through multiple supramolecular interactions.[21–23] Thus, the high efficiency of PLP-assisted transformations suggests that aldimine formation and transimination reactions can be attained under physiological conditions when the system is properly designed. Despite that a handful of studies showed how supramolecular and electronic interactions can be used to increase imine stability,[24–28] the structural features to favour aldimine over the competing hydrate formation in water have been quite overseen.

Herein we report a successful approach to increase imine yields while preventing the hydration of the aldehyde by taking advantage of the supramolecular, electronic, and steric preferences of each reaction component (aldehyde, amine, hydroxide/water), intermediate (hemiaminal), and product (hydrate, imine, iminium). Besides, the best-performing aldehyde acts as an inhibitor of the glutamic-pyruvic transaminase likely through dynamic aldimine exchange with the **PLP** cofactor.

## Results and discussion

One notes that increasing the electrophilic character of the aldehyde (*e.g.*, electron-withdrawing substituents) is the most

*Laboratoire de Chimie Supramoléculaire, Institut de Science et d'Ingénierie Supramoléculaires (ISIS), Université de Strasbourg, 8 allée Gaspard Monge, Strasbourg, 67000, France. E-mail: estevefranch@unistra.fr; lehn@unistra.fr*

† Electronic supplementary information (ESI) available: Experimental section, main text support figures and tables, copies of $^1$H, $^{13}$C NMR, and HRMS spectra, DFT cartesian coordinates. See DOI: https://doi.org/10.1039/d4sc02206h

commonly used method to increase imine yields. However, this approach also favours the $H_2O$ addition to the activated carbonyl that generates the hydrate, decreasing the aldimine selectivity (Fig. 1A). We envisaged that the introduction of negatively-charged bulky groups near the carbonyl unit may disfavour the hydrate formation due to electrostatic repulsions

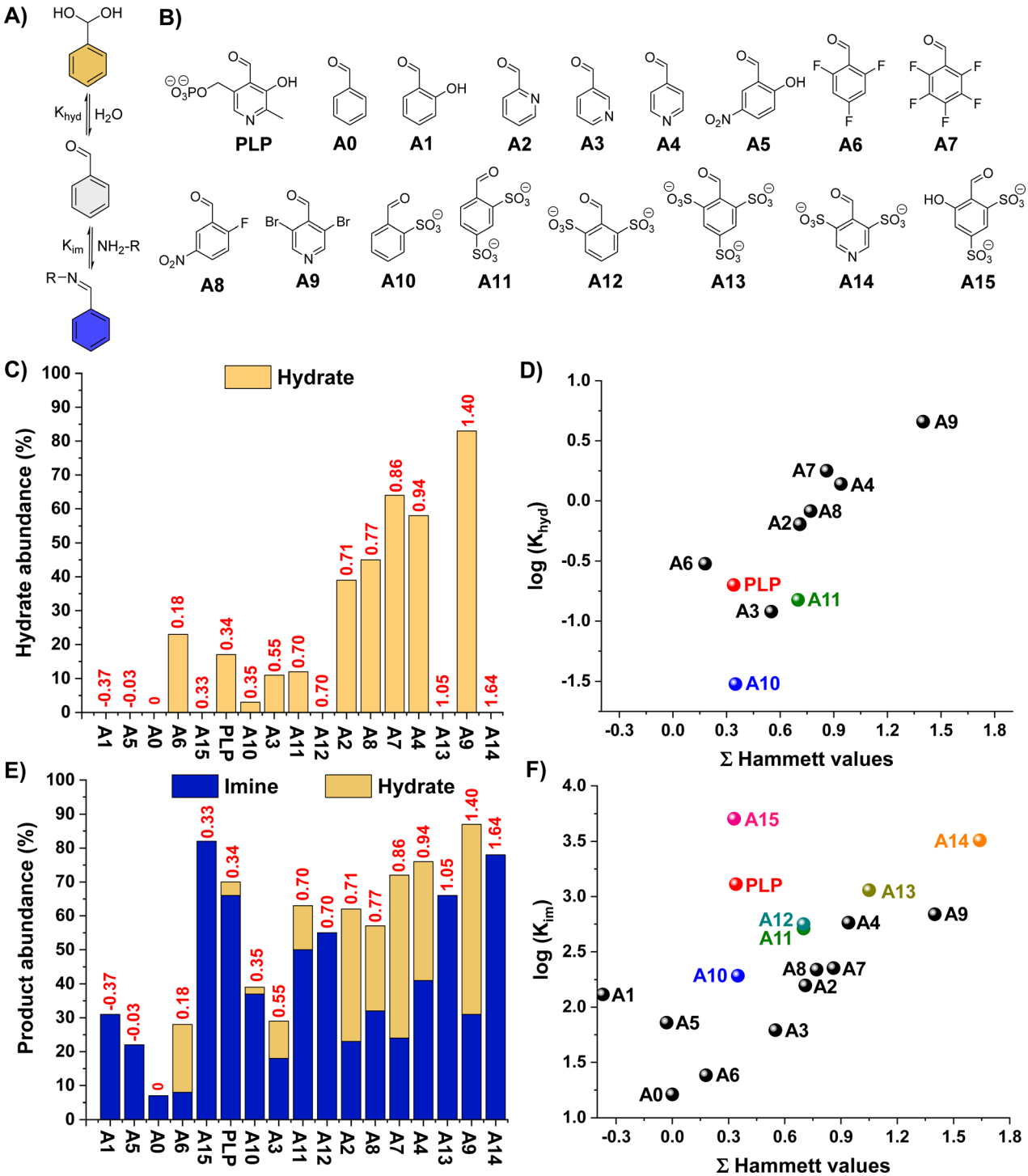


Fig. 1 (A) Hydration and imine formation equilibrium. (B) Chemical structures of the aldehydes studied in this work (C) hydrate abundances (%) and (D) Hammett plot of the log($K_{hyd}$) for the different aldehydes. $K_{hyd}$ for **A1**, **A5**, **A0**, **A12**, **A13**, **A14** and **A15** could not be calculated because no hydrate was detected. (E) Hydrate-imine product abundances (%) and (F) Hammett plot of the log($K_{im}$) for the reaction between the aldehydes and **B1**. The results have been sorted with increased ΣHammett scores (red values in C and E). Results for **PLP** and aldehydes of major interest have been coloured. Hydration reaction conditions: 5 mM aldehyde, $D_2O$, pD 7.0 (50 mM PBS), 295 K, 1 h. Imination reaction conditions: 5 mM aldehyde and 5 mM **B1**, $D_2O$, pD 7.0 (50 mM PBS), 295 K, 3 h. Product abundances determined by $^1$H NMR spectroscopy (500 MHz, 295 K). Error in NMR measurements: 5%.

and crowding effects. Accordingly, sulfonate groups were selected, also taking into account their electron-withdrawing character that could further favour imine formation.

The propensity of a series of benzaldehyde derivatives (**AX**, Fig. 1B) and **PLP** to form hydrates was first assayed in $D_2O$ (5 mM aldehyde, pD 7.0, 50 mM PBS). Aldehydes **A12–A15** were then synthesized in one-step following reported procedures (see ESI† for details).[29] The Hammett plot of the apparent hydration equilibrium constants ($K_{hyd}$) showed the expected increase in hydrate formation for the aldehydes containing more electron-withdrawing substituents (higher Hammett values) with a slope of 1.7 (*e.g.*, **A0** < **A6** < **A2** < **A8** < **A4** < **A9**, Fig. 1C and Table S1;† see also Fig. 1D),[30,31] in good agreement with previous reports.[32] Interestingly, however, the species containing two sulfonate groups in *ortho*-position led to significantly lower $K_{hyd}$ than aldehydes with similar Hammet values (see for instance **A11** *vs.* **A2** in Fig. 1D), suggesting a destabilizing effect of these negatively-charged bulky groups towards hydrate formation. The effect of pD on the aldehyde hydration was also assessed. Dissolving the aldehydes at pD 0.6 resulted in the expected increase in hydrate formation for **PLP**, **A2**, **A3**, **A4**, and **A9** due to the protonation of their pyridine nitrogen site (Fig. S1†). In contrast, pyridinium **A14** was barely hydrated under these conditions despite its great Hammett score (3.27), stressing that the sulfonate groups were disfavouring aldehyde hydration. The hydrate abundance of the other aldehydes did not significantly change at such acidic pD. An increase in the pD of the solution to 10.6 led to minor differences when compared to the results obtained at pD 7.0 (Fig. S2†). At pD 13.6, hydrate abundances ≥95% were obtained for **A2**, **A3**, **A4**, **A6**, **A7**, **A8**, and **A9** (Fig. S3†), but no hydration was observed for **PLP**, **A1**, **A5**, and **A10–A15**, corroborating the key role of bulky and/or negatively-charged *ortho*-substituents in preventing hydrate formation.

We then screened the imine formation reactions by studying the apparent equilibrium constants ($K_{im}$) for the cholamine chloride (**B1**) addition to the different aldehydes, since its terminal $-NH_2$ group is barely protonated at such pD.[33] In general, the $K_{im}$ increased with higher Hammet scores. Notwithstanding, the non-linearity of the results gave insight into the key structural features to favour imines over hydrates (Fig. 1E and F, see also Fig. S4 and S5†):

(i) Aldehydes with small and neutral electron-withdrawing groups (*i.e.*, **A2–A4**, **A6–A9**) do not effectively form imines due to significant competing hydrate formation (Fig. 1F; see also grey fitting in Fig. S5†).

(ii) Aldehydes with bulky and negatively-charged *ortho*-substituents (*i.e.*, **A10–A14**) barely form hydrates and give high $K_{im}$, leading to remarkable imine-to-hydrate selectivities (Fig. S4;† see also brown fitting in Fig. S5†). In addition, these negative groups might also be involved in the stabilization of the potential iminium cations through attractive electrostatic interactions and H-bonding.[22]

(iii) Salicylaldehyde derivatives (*viz.* **A1**, **A5** and **PLP**) promote relatively high $K_{im}$ despite their low Hammett values of −0.37, −0.03 and 0.34, respectively (Fig. 1F; see also yellow fitting in Fig. S5†).[34] This behaviour is ascribed to the presence of intramolecular H-bonding and electrostatic forces that stabilize the aldimine/aldiminium.[20,22,23,35]

(iv) The combination of (ii) and (iii), as in the case of **A15**, leads to the highest $K_{im}$ with excellent aldimine selectivities (Fig. 1F and S4†).

One notes that the abundance of hydrate and imine when using aldehydes with small and neutral electron-withdrawing groups is rather similar, indicating that the difference in energies of formation for such products is small (*e.g.*, **A9**, **A4**, **A7**, **A8**). On the other hand, this energy difference is much greater in favor of the imine/iminium for aldehydes containing *ortho*-substituents that can stabilize such aldimine/aldiminium bonds by means of supramolecular interactions (see for instance DFT section below).

The $K_{im}$ dependence on the pD was also assayed to evaluate the applicability of the sulfonate-containing aldehydes at different pH ranges. Remarkably, the $K_{im}$ for **A15** was almost 10-times higher than that of **PLP** all over the biologically-relevant pD range (*i.e.*, 6.5–7.8), with imine abundances >90% (Fig. S6†). At lower pD values (<5.5), the addition of **B1** to the different aldehydes was hampered by the complete protonation of the terminal $-NH_2$ of the amine (Fig. S7 and S8†). As expected, higher pD decreased the protonation of **B1** and resulted in greater $K_{im}$ for **A0**, in agreement with previous reports.[23] In contrast, aldehydes containing sulfonate (*viz.* **A10**, **A12**, **A13**, **A13** and **A15**) and/or phenolate (**A1**, **A5**, **PLP** and **A15**) units in *ortho*-position showed a decrease in imine formation at pD > 8.5 (Fig. S7 and S8†). We hypothesized that these findings could be related to the iminium/imine equilibrium and its effect on the dynamic covalent reaction. The high $\delta$ values (>8.6 ppm) observed for the –CH=N– signals of these aldehydes suggested the presence of the corresponding iminium cations, in line with reported results.[23] We thus attempted to determine the $pK_a$ of the iminium cations ($pK_{a,iminium}$) by $^1$H-NMR spectroscopy through the $\delta$ changes in the –CH=N– signal (Fig. S9†). However, the only species that experienced a significant shift in the –CH=N– signal were **A5** and **PLP**/**A15**, giving $pK_{a,iminium}$ values of *ca.* 8 and 10.5, respectively. For these aldehydes, the $K_{im}$ drastically dropped once the pD of the solution overtook their $pK_{a,iminium}$, suggesting a much higher thermodynamic stability of the iminium cations over that of the imines. In contrast, the –CH=N– signal for the **B1**-condensation products with the aldehydes **A10**, **A11**, **A12**, **A13** and **A14** barely shifted even at quite high pD, but their $K_{im}$ still decreased to almost 0. Hence, we rationalized that the pD value where the $K_{im}$ dropped corresponded to the $pK_{a,iminium}$, and that the stability of the unprotonated imines must be lower than those of **PLP** and **A15**, as no NMR shift indicative of imine formation was observed at pD > $pK_{a,iminium}$.

DFT calculations were performed for the hydrate, hemiaminal, imine and iminium derived from **A12** (sulfonate groups in both *ortho*-positions) to shed light on the iminium-to-hydrate selectivity observed experimentally (Fig. 2A). The energetic profiles showed endergonic processes for the formation of the species presenting a $Csp^3$ hybridization: hydrate and hemiaminal. This indicated that the sterically-crowded microenvironment of the carbonyl unit preferred a $Csp^2$ planar

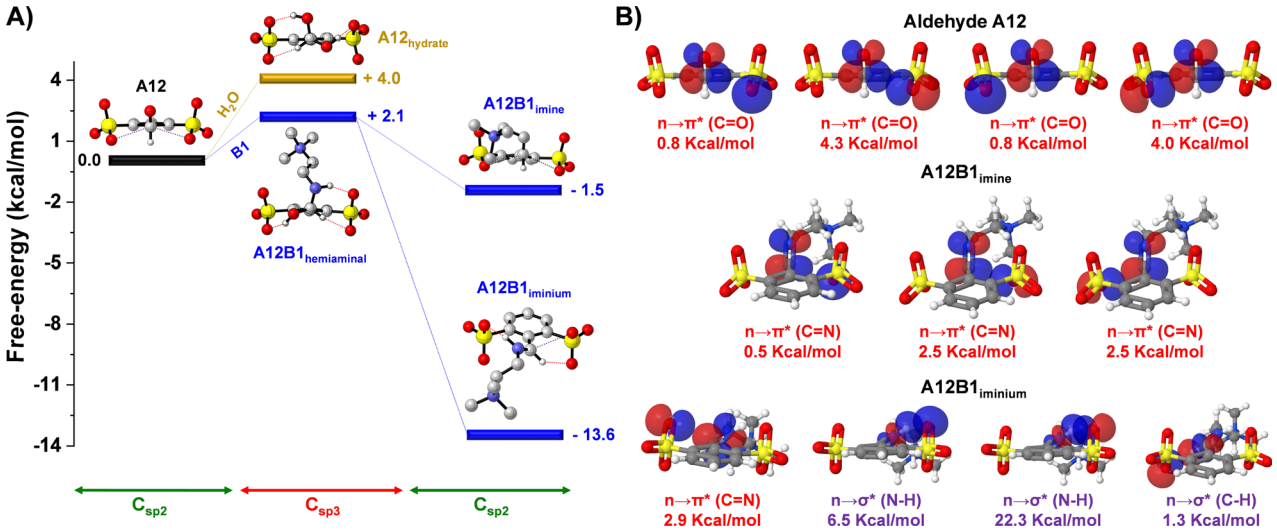


Fig. 2 (A) DFT calculated energy profile (b3lyp/6-311g(d,p), PCM = water) for the generation of the intermediate -hemiaminal- and product -hydrate, imine and iminium-of the reaction between **A12**-$H_2O$ (yellow)/**A12**–**B1** (blue). Discontinuous lines in red and purple show the H-bonds and $n \rightarrow \pi^*$ interactions, respectively. (B) Optimized structures of **A12**, imine **A12B1** and iminium **A12B1**, with NBOs and energies (kcal $mol^{-1}$) listed.

conformation rather than the bulkier $Csp^3$ tetrahedral configurations of the hydrate and hemiaminal.[36] The preference for C–O *vs.* C–N release/cleavage from the tetrahedral intermediates may also involve stereoelectronic effects.[37,38] Whereas the imine **A12B1** presented a subtly exergonic free energy of formation ($-1.5$ kcal $mol^{-1}$), a much stronger stabilization was observed on generation of the iminium derivative ($\Delta G = -13.6$ kcal $mol^{-1}$), in accordance with the experimental results. Such exergonic energies were assigned to the recovery of the sterically-suitable $Csp^2$ hybridization in the **A12–B1** condensation products, with additional electrostatic, H-bonding and $n \rightarrow \pi^*$ interactions stabilizing the iminium cation.[27,39]

The role of the $n \rightarrow \pi^*$ and H-bond interactions was further studied through natural bond orbital (NBO) analyses to estimate the interaction energies according to second-order perturbation theory ($\Delta E^{(2)}$).[26] Two oxygen lone pairs of each of the sulfonate groups (4 lone pairs in total) were overlapping with the antibonding orbital of the carbonyl group in **A12**, with NBO energies of 0.8, 4.3, 0.8 and 4.0 kcal $mol^{-1}$ ($n \rightarrow \pi^*$ (C=O) in Fig. 2B; see also Table S2†). The sum (9.9 kcal $mol^{-1}$) was significantly higher than the one observed for the sulfonate-imine $n \rightarrow \pi^*$ (C=N) interactions (sum = 5.5 kcal $mol^{-1}$). These values are in agreement with the aldehydes being better electron acceptors than their imines. A different scenario was found for the **A12B1** iminium cation. This species was mainly stabilized by a strong hydrogen bonding between the sulfonate group and the acidic proton of the iminium unit ($n \rightarrow \sigma^*$ (N–H) = 28.8 kcal $mol^{-1}$), together with a weaker H-bond between the iminium CH and the lone pair of the other *ortho*-sulfonate substituent ($n \rightarrow \sigma^*$ (C–H) = (1.3 kcal $mol^{-1}$)), which also contributed through a sulfonate-iminium $n \rightarrow \pi^*$ (C=N) interaction (2.9 kcal $mol^{-1}$). Therefore, the low $K_{im}$ observed for the sulfonate-containing species at high pD values (pD > $pK_{a,iminium}$) was likely the result of the stronger $n \rightarrow \pi^*$ interactions for the aldehyde than for the imine derivatives that shifted the equilibrium back to the reagents once the iminium could not be generated.

We envisaged that such bulky and negatively-charged substituents near the electrophilic site might also affect the kinetic preferences of the products.[40,41] The steric hindrance of the carbonyl unit was estimated using the SambVca web server, which calculates buried volumes and steric maps (Fig. 3A; see ESI† for details).[42,43] Results suggested a remarkably sterically-hindered microenvironment for species presenting sulfonate groups in both *ortho*-positions, namely **A12**, **A13** and **A14**, which should experience slower nucleophilic additions. In fact, the CHO buried volumes for such aldehydes represented *ca.* 27% of the total space, providing $a \approx$ 9-fold increase in comparison with the value calculated for **A0** (3%, Fig. 3A). In terms of the imine/iminium formation, $^1$H NMR monitoring over time revealed slower rates for the reaction between **B1** and **A12**/**A13**/**A14**, needing *ca.* 3 h to reach the equilibrium state (Fig. 3B). In contrast, aldehydes with CHO buried volumes <20% (*i.e.*, **PLP**, **A10**, **A11**, **A15**) attainted the equilibrium in less than 10 min, in good accordance with the expected fast imitation reactions in water.[12]

Concerning the aldehyde hydration, the kinetic profiles were too fast to be measured due to the huge excess of $H_2O$ present in the media. Yet, one should note that the presence of strong electrostatic repulsions between the electron-rich O atom of the $OH^-/H_2O$ and the negatively-charged sulfonate groups may slow down the generation of the hydrate, but without affecting the thermodynamic outcome. Electron density surfaces (EDS) of the aldehydes (**A10–15**, **PLP**) and nucleophiles ($H_2O$, $OH^-$, **B1**) were calculated to evaluate this assumption (Fig. 3C). In the case of the nucleophiles, the electron density of $OH^-$ -and to a lesser degree $H_2O$– was substantially more negative than that of **B1**, in line with the number of lone pairs present in the nucleophilic site (3 for $OH^-$, 2 for $H_2O$ and 1 for **B1**). On the other hand, the negative electron density surrounding the aldehydes increased in the order: **A10** ≈ **PLP** < **A11** ≪ **A15** < **A12** ≈ **A14** < **A13**.

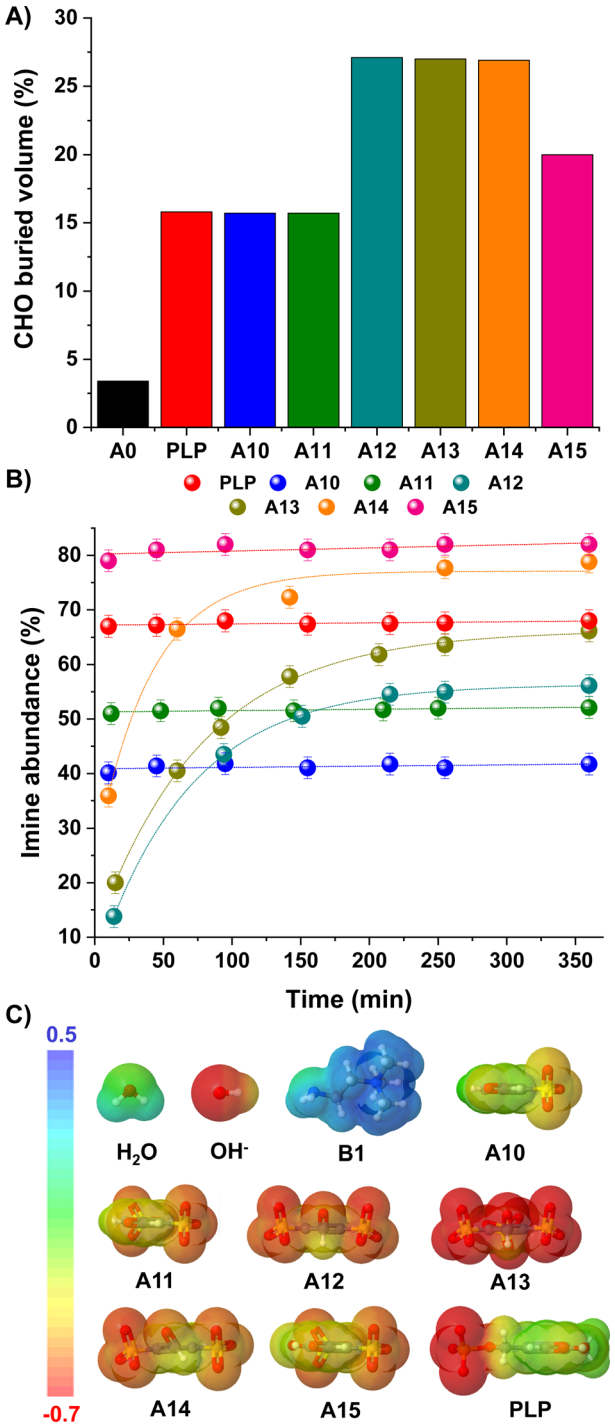


Fig. 3 (A) Buried volumes (%) calculated for the carbonyl group of aldehydes **A0**, **PLP**, **A10**–**A15**. Values calculated using SambVca web server (see ESI†).[42,43] (B) Kinetic profiles for the imine formation reaction between **B1** and aldehydes **PLP** and **A10**–**A15**. Imine abundances (%) determined by $^1$H NMR spectroscopy (500 MHz, $D_2O$, pD 7.0, 50 mM PBS, 295 K). Concentration: 5 mM for each component. (C) EDS (b3lyp/6-311g(d,p), PCM = water) for aldehydes **A10**–**15**/**PLP** and nucleophiles $H_2O$/$OH^-$/**B1**. The isosurface density values range from −0.7 to 0.5 a.u. in all cases.

The imine formation dependence on the protonation state of the amines was then evaluated for the best-performing aldehydes **PLP**, **A14** and **A15**. Results for **A14** revealed a drastic decrease in $K_{im}$ upon reaction with amines containing <10% unprotonated –$NH_2$ groups at pD 7.0 (see orange bars for **B3**, **B4**, **Val** and **B5**, Fig. 4).[33] For example, **A14** did not react with **Val** and **B5**, and imine yields of *ca.* 10% were attained with **B3** and **B4** (p$K_a$ values of 9.1 and 9.6, respectively; see Fig. S10 and Table S3†). In contrast, aldehyde **A15** gave high imine abundances even when reacted with amines presenting a p$K_a$ value >10 (*e.g.*, **B5**). In a similar manner, **PLP** was able to react with such amines despite the high degree of protonation of the –$NH_2$ groups at physiological pH, suggesting that the *ortho*-OH group must be activating the amines for their nucleophilic attack.[44] To our delight, **A15** was able to render higher $K_{im}$ than **PLP** in all cases, stressing its remarkable reactivity (Fig. 4). Moreover, the stability of **PLP**-derived imines was lower than that of **A15**, as evidenced by the appearance of side-product signals in the $^1$H NMR spectrum of **PLPB1** after 120 h (Fig. S11 and S12†). The imitation reactions of **A14**, **A15** and **PLP** with **Lys**-derivatives were also assayed. As predicted, aldehyde **A14** was only able to react with the Nα of **LysOMe** due to its relatively low –$NH_2$ protonation at pD 7.0 (50%, Fig. S13†),[13,45] not forming any imines with the Nε of **Lys** and **LysOMe** nor with the Nα of **Lys** (unprotonated –$NH_2$ < 2%, Table S3; Fig. S14†). On the other hand, both **PLP** and **A15** reacted with the Nα and Nε of **LysOMe** and **Lys**, with a slightly preferential aldimine formation at the Nα in both cases. The reaction with Nε was further corroborated

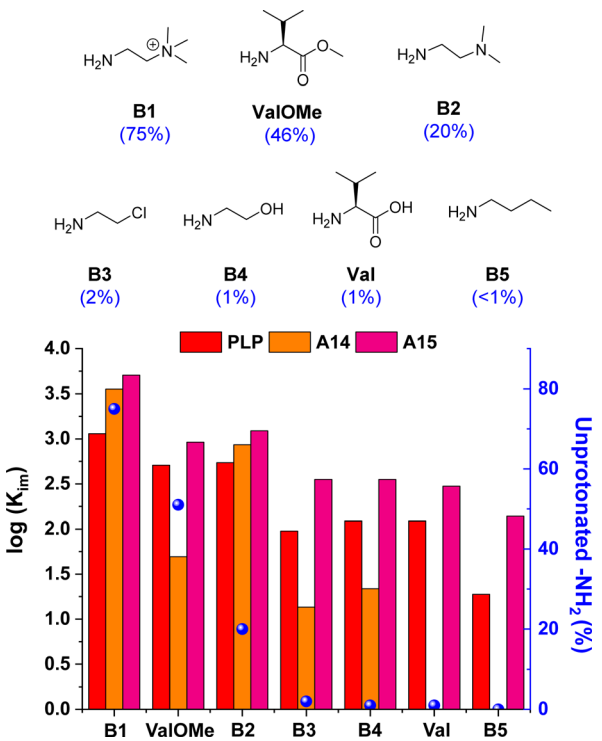


Fig. 4 Chemical structures (above) and log $K_{im}$ (below) for the amine screening using **PLP**/**A14**/**A15**. Component abundances determined by $^1$H NMR spectroscopy (500 MHz, $D_2O$, pD 7.0, 50 mM PBS, 295 K). Concentration: 5 mM for each component. The numbers in brackets correspond to the unprotonated –$NH_2$ group at pD 7.0. See Table S3† for p$K_a$ and protonation degree of amines. See Fig. S7† for imine abundances (%).

using **AcNαLysOMe** as the nucleophile, observing that only **PLP** and **A15** gave aldimines.

The dynamic character of **A15**-derived aldimines was also evaluated with a simple re-arrangement experiment, observing that when **B1** (5 mM final concentration) was introduced into a solution containing **A15B5** (5 mM mixture of **B5** and **A15**), **B5** was released and **A15B1** was formed as the major product (Fig. S15†). This aldimine interconversion occurred instantaneously in the time range of the experiment, stressing the outstanding reversibility of **A15**-derived aldimines under physiological conditions.

All these results paved the way for studying the regulation of a **PLP** dependent enzyme (*i.e.*, Glutamic-Pyruvic Transaminase from porcine heart, **GPT**) with aldehyde **A15**.[46–50] **GPT** is catalytically-active in amino acid-$D_2O$ exchange reactions in the presence of pyruvate under slightly basic conditions.[51] Thus, we studied the L-alanine-$D_2O$ exchange reaction in an NMR tube containing L-alanine (90 mM), pyruvate (1.5 mM), potassium phosphate buffer (100 mM, pD 7.8) and 7 units of **GPT** (*ca.* 1 μM). The reaction course was easily followed by $^1$H NMR observing the deuterium exchange of both α and β hydrogens of L-alanine (black points in Fig. 5A; see also Fig. S16†). The experiment in the absence of **GPT** showed no reaction (grey points in Fig. 5A). As expected, the addition of a large excess of **PLP** and **A14** did not change the catalytic activity of **GPT** (red and orange points in Fig. 5A, respectively), since **PLP** is already present as the cofactor and **A14** does not form imines with Nε-**Lys** (see Fig. S13†). In contrast, 200 eq. of **A15** triggered a remarkable inhibition of the enzyme (*ca.* 90%). Although lower amounts of **A15** led to a less efficient inhibition, the $IC_{50}$ for this aldehyde was about 15 μM (*ca.* 15 eq). To support that the inhibition observed was indicative of **A15-PLP** aldimine exchange, we studied the amount of **A15** required to replace **PLP** from the preformed **PLPAcNαLysOMe** aldimine under related experimental conditions (pD 7.8). The presence of 0.7 eq. of **A15** resulted in a significant **PLP** replacement (42%), but 4 eq. of **A15** were needed to reach an aldimine exchange >90% (Fig. S17†). The higher number of equivalents needed to replace **PLP** by **A15** in the active site of **GPT** was assigned to a supramolecular mismatch between the *para*-sulfonate group of **A15** and the carboxylate group of the aspartic acid residue (see Fig. S18† for the example of an analogous PLP-complex of the Human alanine aminotransferase 2, PDB: 3IHJ).

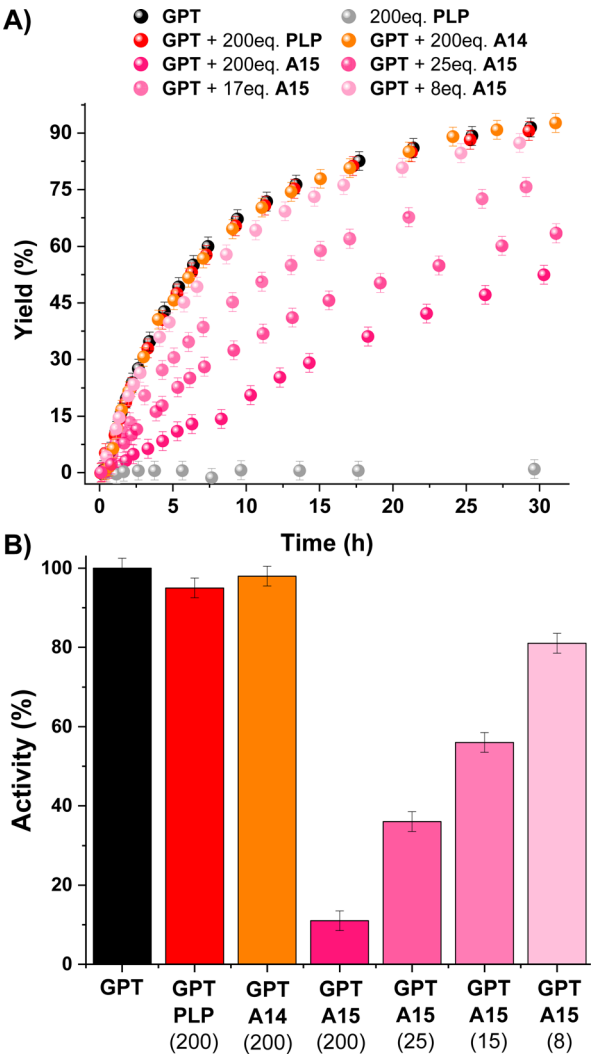


Fig. 5 (A) Kinetic profiles for the L-alanine-$D_2O$ exchange reactions. Colour code: black (GPT + pyruvate), grey (PLP + pyruvate), red (GPT + PLP + pyruvate), orange (GPT + A14 + pyruvate), pink (GPT + A15 + pyruvate). (B) GPT activity observed for the different inhibition experiments. Black column corresponds to the neat GPT activity. Number in brackets describe the equivalents of the aldehydes introduced (also the concentration in μM). Reaction conditions: $D_2O$, pD 7.8, 100 mM PBS, 295 K. Concentrations: L-alanine (90 mM), pyruvate (1.5 mM), GPT (1 μM).

## Conclusions

In conclusion, we have evaluated the hydration and imitation reactions of different aldehydes in aqueous media, comparing the results with the ones attained in the presence of the biologically-relevant **PLP**. Aldehydes **A12–A15** resulted in remarkable $K_{im}$ with complete silencing of hydrate formation ($K_{hyd}$) when reacted with **B1**, despite the low concentrations employed. The mode-of-action to attain excellent imine *vs.* hydrate selectivities relies on the interplay between: (i) high Hammett values to increase carbonyl electrophilic character; (ii) sterically crowding units to disfavour the $Csp^2$ hybridization of hydrate and hemiaminals; and (iii) negatively-charged sites to stabilize the iminium cations through electrostatic, H-bonding and $n \rightarrow \pi^*$ interactions. The imine yields for the reaction between the best-performing aldehydes (*i.e.*, **PLP**, **A14** and **A15**) and amines presenting a high $-NH_2$ protonation were also evaluated. The results obtained in the presence of **A15** surpassed the ones of **PLP**, postulating **A15** as the most active aldehyde in imitation reactions under physiological conditions reported to date. In addition, **A14** can be used for the selective Nα functionalization of peptides since it does not react with the Nε of **Lys**-derivatives.

Preliminary studies on the **A15** conjugation to a model protein suggested the suitability of this aldehyde to replace **PLP** from the active site through dynamic aldimine exchange, allowing for the inhibition of the enzymatic activity. All these

results, taken together, will facilitate the application of imine chemistry in water, with a particular interest in the bio-orthogonal modification of proteins with dynamic covalent bonds.

## Data availability

The authors confirm that the data supporting the findings of this study are available within the ESI.† Additional experimental data are available on request from the corresponding author (F. E.).

## Author contributions

The manuscript was written through contributions of all authors. All authors have given approval to the final version of the manuscript. Conceptualization: F. E. and J. M. L. Data curation: F. E. and T. R. Formal analysis: F. E. Funding acquisition: J. M. L. Investigation: T. R. (supporting) and F. E. (lead). Methodology: F. E. Project administration: J. M. L. Resources: J. M. L. Supervision: F. E. and J. M. L. Validation: F. E. Visualization: T. R. (supporting) and F. E. (lead). Writing – original draft: F. E. Writing – review and editing: T. R. (supporting), F. E., and J. M. L.

## Conflicts of interest

There are no conflicts to declare.

## Acknowledgements

This work was supported by the ERC (Advanced Research grant SUPRADAPT 290585), the University of Strasbourg Institute for Advanced Study (USIAS), and Fondation Jean-Marie Lehn. F. E. acknowledges Fundación Ramón Areces for a postdoctoral fellowship. T. R. thanks the CSC Graduate School funded by the French National Research Agency (CSC-IGS ANR-17-EURE-0016) for a PhD fellowship. The authors thank Dr J. L. Schmitt, Dr G. Ragazzon, Dr A. Osypenko, Dr Z. Yang, Dr S. Jung, B. Kozibroda, M. J. Aguilera, and C. Antheaume for helpful discussions.

## Notes and references

1 M. R. Belowich and J. F. Stoddart, *Chem. Soc. Rev.*, 2012, **41**, 2003–2024.
2 K. Geng, T. He, R. Liu, S. Dalapati, K. T. Tan, Z. Li, S. Tao, Y. Gong, Q. Jiang and D. Jiang, *Chem. Rev.*, 2020, **120**, 8814–8933.
3 J. Yu, M. Gaedke and F. Schaufelberger, *Eur. J. Org Chem.*, 2023, **26**, e2022011.
4 J.-M. Lehn, *Angew. Chem., Int. Ed.*, 2015, **54**, 3276–3289.
5 K. Acharyya, S. Mukherjee and P. S. Mukherjee, *J. Am. Chem. Soc.*, 2013, **135**, 554–557.
6 Y.-Q. Zou, D. Zhang, T. K. Ronson, A. Tarzia, Z. Lu, K. E. Jelfs and J. R. Nitschke, *J. Am. Chem. Soc.*, 2021, **143**, 9009–9015.
7 Z. Yang, F. Esteve, C. Antheaume and J.-M. Lehn, *Chem. Sci.*, 2023, **14**, 6631–6642.
8 M. Ovalle, M. Kathan, R. Toyoda, C. N. Stindt, S. Crespo and B. L. Feringa, *Angew. Chem., Int. Ed.*, 2023, **62**, e202214495.
9 A. Seoane, R. J. Brea, A. Fuertes, K. A. Podolsky and N. K. Devaraj, *J. Am. Chem. Soc.*, 2018, **140**, 8388–8391.
10 S. P. Afrose, C. Mahato, P. Sharma, L. Roy and D. Das, *J. Am. Chem. Soc.*, 2022, **144**, 673–678.
11 F. Esteve, B. Altava, E. García-Verdugo, S. V. Luis and J.-M. Lehn, *Chem*, 2022, **8**, 2023–2042.
12 C. Godoy-Alcántar, A. K. Yatsimirsky and J.-M. Lehn, *J. Phys. Org. Chem.*, 2005, **18**, 979–985.
13 F. Esteve, F. Rahmatova and J.-M. Lehn, *Chem. Sci.*, 2023, **14**, 10249–10257.
14 Y. Lei, Z. Li, G. Wu, L. Zhang, L. Tong, T. Tong, Q. Chen, L. Wang, C. Ge, Y. Wei, Y. Pan, A. C. H. Sue, L. Wang, F. Huang and H. Li, *Nat. Commun.*, 2022, **13**, 3557.
15 Y. Lei, Q. Chen, P. Liu, L. Wang, H. Wang, B. Li, X. Lu, Z. Chen, Y. Pan, F. Huang and H. Li, *Angew. Chem., Int. Ed.*, 2021, **60**, 4705–4711.
16 Y. Chen, Y. Lei, L. Tong and H. Li, *Chem.–Eur. J.*, 2022, **28**, e202102910.
17 K. Meguellati, A. Fallah-Araghi, J. C. Baret, A. El Harrak, T. Mangeat, C. M. Marques, A. D. Griffiths and S. Ladame, *Chem. Commun.*, 2013, **49**, 11332–11334.
18 A. C. Eliot and J. F. Kirsch, *Annu. Rev. Biochem.*, 2004, **73**, 383–415.
19 J. Liang, Q. Han, Y. Tan, H. Ding and J. Li, *Front. Mol. Biosci.*, 2019, **6**, 4.
20 E. F. Oliveira, N. M. F. S. A. Cerqueira, P. A. Fernandes and M. J. Ramos, *J. Am. Chem. Soc.*, 2011, **133**, 15496–15505.
21 W. R. Griswold and M. D. Toney, *J. Am. Chem. Soc.*, 2011, **133**, 14823–14830.
22 J. P. Richard, T. L. Amyes, J. Crugeiras and A. Rios, *Biochim. Biophys. Acta*, 2011, **1814**, 1419–1425.
23 J. Crugeiras, A. Rios, E. Riveiros and J. P. Richard, *J. Am. Chem. Soc.*, 2009, **131**, 15815–15824.
24 S. Jia, H. Ye and L. You, *Org. Chem. Front.*, 2022, **9**, 3966–3975.
25 K. B. Muchowska, D. J. Pascoe, S. Borsley, I. V. Smolyar, I. Mati, C. Adam, G. S. Nichol, K. B. Ling and S. L. Cockroft, *Angew. Chem., Int. Ed.*, 2020, **59**, 14602–14608.
26 H. Chen, H. Ye, Y. Hai, L. Zhang and L. You, *Chem. Sci.*, 2020, **11**, 2707–2715.
27 H. Zheng, H. Ye, X. Yu and L. You, *J. Am. Chem. Soc.*, 2019, **141**, 8825–8833.
28 P. M. S. D. Cal, J. B. Vicente, E. Pires, A. V. Coelho, L. F. Veiros, C. Cordeiro and P. M. P. Gois, *J. Am. Chem. Soc.*, 2012, **134**, 10299–10305.
29 T. Fiala, J. Wang, M. Dunn, P. Šebej, S. J. Choi, E. C. Nwadibia, E. Fialova, D. M. Martinez, C. E. Cheetham, K. J. Fogle, M. J. Palladino, Z. Freyberg, D. Sulzer and D. Sames, *J. Am. Chem. Soc.*, 2020, **142**, 9285–9301.
30 J. H. Blanch, *J. Chem. Soc. B*, 1966, 937–939.
31 C. Hansch, A. Leo and R. W. Taft, *Chem. Rev.*, 1991, **91**, 165–195.
32 R. A. McClelland and M. Coe, *J. Am. Chem. Soc.*, 1983, **105**, 2718–2725.

33 Note: 75% of unprotonated $-NH_2$ group for **B1** at pH 7.4. Value calculated using Marvin JS software. See Table S3† for $pK_a$ and protonation degrees of the different amines considered in this work.
34 Note: Hammett values of ionizable groups might change depending on the pH of the solutions. See Table S1† for the different values used in this work.
35 S. M. So, L. Mui, H. Kim and J. Chin, *Acc. Chem. Res.*, 2012, **45**, 1345–1355.
36 J. M. Sayer and W. P. Jencks, *J. Am. Chem. Soc.*, 1977, **99**, 464–474.
37 J.-M. Lehn, G. Wipff and H. B. Bürgi, *Helv. Chim. Acta*, 1974, **57**, 493–496.
38 J.-M. Lehn and G. Wipff, *Helv. Chim. Acta*, 1978, **61**, 1274–1286.
39 C. A. Hunter, *Angew. Chem., Int. Ed.*, 2004, **43**, 5310–5324.
40 Note: The potential proton transfer events (either intramolecular or with the $H_2O$ solvent molecules) occurring during each reaction step hampered the successful characterization of the transition states involved.
41 J. Hine and F. A. Via, *J. Am. Chem. Soc.*, 1971, **94**, 190–194.
42 L. Falivene, Z. Cao, A. Petta, L. Serra, A. Poater, R. Oliva, V. Scarano and L. Cavallo, *Nat. Chem.*, 2019, **11**, 872–879.
43 L. Falivene, R. Credendino, A. Poater, A. Petta, L. Serra, R. Oliva, V. Scarano and L. Cavallo, *Organometallics*, 2016, **35**, 2286–2293.
44 J. P. Richard, T. L. Amyes, J. Crugeiras and A. Rios, *Curr. Opin. Chem. Biol.*, 2009, **13**, 475–483.
45 H. Jiang, W. Chen, J. Wang and R. Zhang, *Chin. Chem. Lett.*, 2022, **33**, 80–88.
46 T. Sahu, M. Chilamari and V. Rai, *Chem. Commun.*, 2022, **58**, 1768–1771.
47 M. Chilamari, N. Kalra, S. Shukla and V. Rai, *Chem. Commun.*, 2018, **54**, 7302–7305.
48 M. M. Zegota, T. Wang, C. Seidler, D. Y. W. Ng, S. L. Kuan and T. Weil, *Bioconjugate Chem.*, 2018, **29**, 2665–2670.
49 L. Purushottam, S. R. Adusumalli, U. Singh, V. B. Unnikrishnan, D. G. Rawale, M. Gujrati, R. K. Mishra and V. Rai, *Nat. Commun.*, 2019, **10**, 2539.
50 L. Purushottam, S. R. Adusumalli, M. Chilamari and V. Rai, *Chem. Commun.*, 2017, **53**, 959–962.
51 U. M. Babu and R. B. Johnston, *Biochem. Biophys. Res. Commun.*, 1974, **58**, 460–466, DOI: **10.1016/0006-291x(74)90387-8**.